Prediction of the individual wave overtopping volumes of a wave energy converter using experimental testing and first numerical model results

L. Victor[1], P. Troch[1] and J.P. Kofoed[2]

[1] Department of Civil Engineering,
Ghent University,
Technologiepark 904, B-9052 Zwijnaarde (Ghent), Belgium
E-mail: Lander.Victor@ugent.be
Peter.Troch@ugent.be

[2] Department of Civil Engineering,
Aalborg University,
Sohngaardsholmsvej 57, DK-9000 Aalborg, Denmark
E-mail: jpk@civil.aau.dk

Abstract

For overtopping wave energy converters (WECs) a more efficient energy conversion can be achieved when the volumes of water, wave by wave, that enter their reservoir are known and can be predicted. A numerical tool is being developed using a commercial CFD-solver to study and optimize the hydrodynamic behavior of overtopping WECs, which includes the prediction of the individual overtopping volumes.

This paper presents the results of experimental model tests that have been carried out to validate the numerical tool for its ability to predict the individual overtopping volumes for a fixed nearshore 2D-structure. First numerical model results are given for a specific test with regular waves, and are compared with the corresponding experimental results in this paper.

Keywords: device control, numerical CFD models, overtopping, experimental model tests.

Nomenclature

q_{avg} = measured average overtopping discharge [m³/s/m]
g = gravity constant = 9.82 m/s²
WG = wave gauge
Q = dimensionless average overtopping discharge [-]
R = dimensionless crest freeboard [-]
H = wave height [m]
T_p = peak period [s]
$T_{m-1,0}$ = spectral period [s] = m_{-1}/m_0
α = slope angle [rad]
Rc = crest freeboard [m]
V = individual volume [l]

ξ_{0p} = Iribarren number based on the peak period = $\dfrac{\tan\alpha}{\sqrt{\dfrac{2\cdot\pi\cdot H_{m0,toe}}{g\cdot T_p^2}}}$

$\xi_{m-1,0}$ = Iribarren number based on the spectral period = $\dfrac{\tan\alpha}{\sqrt{\dfrac{2\cdot\pi\cdot H_{m0,toe}}{g\cdot T_{m-1,0}^2}}}$

Subscripts

1/3 = average of highest 1/3rd
m0 = spectral value (wave height)
toe = at the toe of the structure

1 Introduction

Overtopping wave energy converters are based on wave run-up on a slope and overtopping into a reservoir that is emptied into the sea through a turbine. For this type of WECs, the physical process of wave overtopping determines the efficiency of the energy conversion. When the volume that overtops into the reservoir - wave by wave - is known, the turbine/control strategy can be adjusted accordingly to achieve an optimal efficiency of the device. This requires a time domain approach to predict these overtopping volumes. Not only wave groupiness of the incoming waves has a significant influence on the individual and average overtopping volumes. Also tide level and foreshore – for nearshore fixed structures (e.g. the Seawave Slot-Cone Generator (SSG) developed by the Norwegian company WaveEnergy) - and changing mass distribution due to water in the reservoir(s) and floating level – for off shore floating structures (e.g. the Wave Dragon (WD) developed by Wave Dragon ApS (Denmark)) – are important

© Proceedings of the 8th European Wave and Tidal Energy Conference, Uppsala, Sweden, 2009

parameters in the determination of the overtopping volumes that need further examination.

A numerical tool is under development to investigate and optimize the hydrodynamic behavior of overtopping WECs. This tool should be able to model the overtopping processes accurately. Also, during several stages in the development of this numerical tool, the numerical results need to be validated with the results of the experimental model tests. The initial approach is 2D, for fixed nearshore structures. Accordingly, the numerical tool consists of a numerical wave flume in which a large number of geometries can be tested. Experimental model tests have been carried out in the period August 2008 – October 2008 in a physical wave flume at Aalborg University (AAU) in order to validate the numerical tool for its ability to predict individual overtopping volumes. The chosen geometries and test parameters for this experimental model are discussed in the next section. The numerical tool is being described in section 3.

This paper mainly concerns the results of the experimental validation tests, in particular the individual overtopping volumes. A first comparison with results of the numerical tool is also carried out for a specific test with regular waves.

2 Experimental model – test set-up

The experimental test set-up at AAU for the validation tests is described in detail in [1]. A short summary is given below. A schematic overview of the test set-up is shown in Fig. 1.

The concrete wave flume with dimensions 25.0 m x 1.2 m x 1.0 m (LxBxH) has a piston-type wave maker with a stroke of 0.6 m and is equipped with an active wave absorption system. The bottom of the flume is not horizontal, but has a mild slope of 1:60 over the total length of the flume. This slope can be interpreted as the foreshore for the structure. A simple structure has been chosen for the validation set-up: a smooth slope which leads the overtopped water to a reservoir. The slope consists of two parts. The upper part (slope 2) is made of aluminum, has a fixed slope of 1:1.73 (slope angle α_2 = 30°) and a vertical height of 0.05 m or 0.10 m. The lower part (slope 1) is made of wood, has a fixed vertical height of 0.5 m and a variable slope angle α_1. The length of the wave flume in front of the slope is approximately 20 m. The reservoir and a dry working area are installed at the rear side of the slope.

Table 1 gives an overview of the used geometries with their corresponding slope angle α_1, water depth and crest freeboard. The geometries have been subjected to both regular and irregular waves. The characteristics of the irregular waves are based on a JONSWAP-spectrum with significant wave heights and peak periods occurring in the Danish North Sea (Table 2). The same wave heights and periods have been used for regular waves. A length scale of 1:30 is considered. Tests with two values for the wave groupiness factor have been carried out for the irregular waves.

Geometry	**Slope angle α_1 [°]**	**Water depth at structure [m]**	**Crest Freeboard [m]**
A1	40 (1:1.19)	0.500	0.050
A2	40	0.475	0.075
A3	40	0.450	0.100
B1	40	0.500	0.100
B2	40	0.475	0.125
C1	30 (1:1.73)	0.500	0.050
C2	30	0.475	0.075
C3	30	0.450	0.100
C4	30	0.525	0.025
D1	30	0.500	0.100
D2	30	0.475	0.125
E1	50 (1:0.84)	0.500	0.050
E2	50	0.475	0.075
E3	50	0.450	0.100
E4	50	0.525	0.025
F1	50	0.500	0.100
F2	50	0.475	0.125

Table 1: Test matrix.

Name wave condition	**Wave height (significant) [m]**	**Period (peak) [s]**
W1	0.0333	1.022
W2	0.0667	1.278
W3	0.1000	1.534
W4	0.1333	1.789
W5	0.1667	2.045

Table 2: Wave conditions (scale 1:30).

When combining Table 1 and Table 2, it should be pointed out that both high (typical for dike structures) and low relative crest freeboards (for overtopping WECs) are used for the tests.

The main steps of the technique that is used to measure the average overtopping discharges, are:

- acquiring the time series of the weight of the reservoir using a weighing cell (pumping occurs for large overtopping volumes);
- correcting those time series with the pump characteristic to achieve a cumulative curve (if necessary);
- time-differentiation of the cumulative curve;
- calculating the average of the differentiated curve.

The weigh cell is accurate for small overtopping volumes (that possibly occur even for low-crested structures) – up to 10 g, but its range is sufficiently broad (150 kg) so that large volumes of water are measured as well. Both the starting level for pumping and the duration of pumping are determined by the allowable water level decrease in the wave flume, by the size of the reservoir, the pump characteristic and by the maximum capacity of the weighing cell. An accurate calibration of the water mass inside the

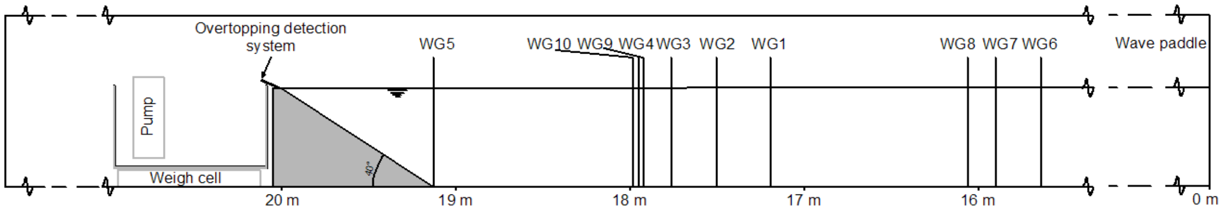

Figure 1: Schematic overview of test set-up for α_1 = 40°.

Figure 2: Front view of experimental set-up.

Figure 3: View of experimental set-up from the back.

Figure 4: Detailed view of overtopping detection system and pump inside reservoir.

reservoir is carried out to take into account the displacement of the pump when it is immersed in the water. A wooden flume has been built centrally inside the concrete flume to minimize the influence of cross waves and the impact of the pumped water on the incoming waves (pump outlet was put in one of the side sections of the wooden flume). This set-up reduces the width of the model to 0.5 m. Nonetheless, during the first tests, some cross waves appeared in the concrete flume outside the wooden flume. Therefore, the active wave absorption system was not switched on during the tests that are used for validation. Cross waves did not occur inside the wooden flume.

The technique described above has been refined in order to determine individual overtopping:

- the reservoir is positioned directly behind the crest of the slope. As a consequence, the time delay between overtopping and reaching the weight detection system is very small. Individual overtopping events should then be clearly visible in the signal of the weigh cell;
- an overtopping detection system (two vertical metal wires acting as a switch) is mounted on the crest of the slope. This system enables identification of the positions on the time axis for which overtopping occurs.

Ten resistive-type wave gauges are positioned inside the wooden flume to determine the water surface elevations at several positions (Fig. 1), the change in wave spectrum and the presence of cross waves inside the wooden flume. Reflection coefficients are calculated using the method of Mansard and Funke [2]. The software program WaveLab (AAU) is used for the data acquisition and the wave analysis. Some pictures of the test set-up are given in Fig. 2, Fig. 3 and Fig. 4.

3 Numerical model – test set-up

The numerical tool is described in detail in [1]. Again a short summary is given below.

The numerical wave flume is developed in FLOW3D® [3], a general applicable CFD-solver, which is based on the Navier-Stokes equations and incorporates a Volume Of Fluid (VOF) method to track the free surface. Customization of the source code is possible to some extent. The following components have been added in order to model the numerical wave flume:

- wave generation: internal mass source (source 1) wave generation for regular, irregular, linear and non-linear waves;
- wave absorption: implementation of a numerical sponge layer in front of reflecting walls by using an additional drag coefficient that is a function of the position inside the sponge layer.

Details on both components can be found in [1]. The basic scheme for the numerical wave flume is shown in Fig. 5. When the waves overtop the structure, the water level in front of the structure will decrease, while water

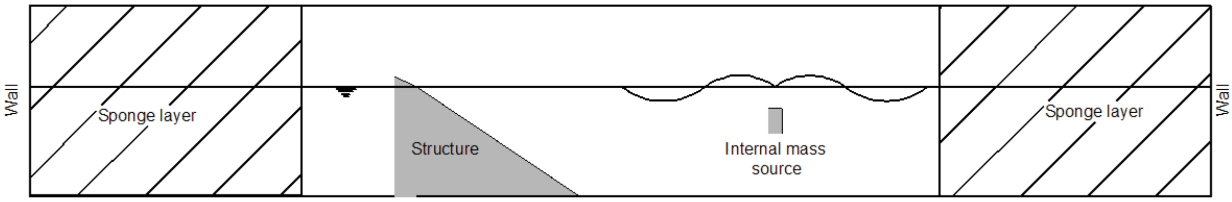

Figure 5: Basic scheme of numerical wave flume.

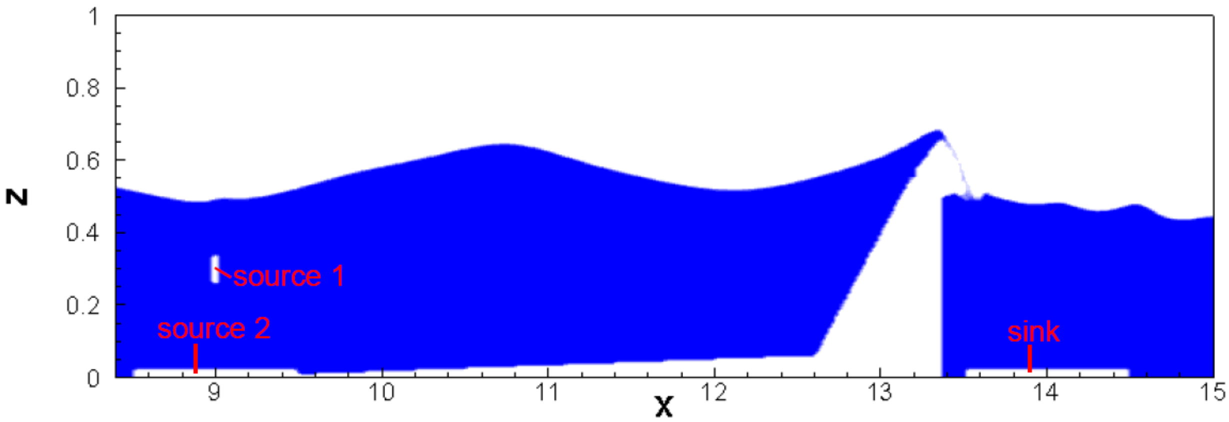

Figure 6: Numerical wave flume – geometry B1-W3.

is added behind the structure. For every wave that overtops the structure, the same amount as the overtopped volume should be added to the water in front of the structure. In the experimental model a pump is used to realize this correction. Numerically, another technique should be used. The correction is enabled by using a mass source (source 2). This source could be installed at the bottom of the flume below the mass source that is responsible for generating the waves as is shown in Fig. 6. The mass source rate of the correction source should be linked to the time-dependent volume of water that overtops the structure.

Geometries used in the experimental model tests can be assembled with standard geometry components available in the numerical model. Wave data from wave gauges in front of the structure can be used for the mass source wave generation.

4 Experimental model – results average discharges

Before determining the individual overtopping volumes for the experimental model tests, their average overtopping discharges are calculated and compared with empirical formulae found in literature [4 – 5]. These overtopping formulae express a dimensionless average overtopping discharge Q as a function of a dimensionless crest freeboard R (relative freeboard height). Both definitions of R and Q contain an incident wave height H at the toe of the structure. Originally, $H_{1/3}$ – i.e. the average of the 1/3rd largest waves - was used for H [6] based on deep water tests. However, after tests carried out with shallow foreshores (non-Rayleigh distributed waves) [7], the spectral wave height H_{m0} (determined for the complete spectrum, including the low-frequent energy) is taken for H instead. The same wave height is used by [4]. As the bottom of the wave flume at AAU is not horizontal, the waves in front of the structure are not Rayleigh distributed. On average, the ratio between H_{m0} and $H_{1/3}$ equals 1.04. Following [7] and [4], the incident H_{m0} at the toe of the structure ($H_{m0,toe}$) is used in the definitions of Q and R. The definitions of Q and R and the overtopping formulae depend on the Iribarren number (ξ_{0p}-values). As ξ_{0p} is larger than 2 for all tests (average slopes are calculated according to the rules of the CLASH database [8]), the formulae for non-breaking waves can be used, with corresponding definitions for R and Q: $R = \dfrac{R_c}{H_{m0,toe}}$ and $Q = \dfrac{q_{avg}}{\sqrt{g \cdot H^3_{m0,toe}}}$. The crest freeboard R_c is measured from the test set-up and its values are given in Table 1. The measured average overtopping discharge q_{avg} is determined from the signal of the weigh cell as explained in section 2.

The empirical (Q,R)-formula mentioned in [4] for smooth slopes and non-breaking waves that is used for comparison with measurements is given below (for the tests discussed here, all γ-factors are equal to 1).

$$Q = 0.2 \cdot \exp(-2.6 \cdot R) \qquad (1)$$

with $\xi_{m-1,0}$ <5, $0.6 \le R \le 3.5$ and $(\cot\alpha)_{\min} = 1$ (α being the angle of the slope, $\xi_{m-1,0}$ is the Iribarren number based on the spectral wave period $T_{m-1,0} = m_{-1}/m_0$)

An extension of this formula for lower relative crest freeboards is given in [5] for the case of overtopping

WECs. [5] proposes to apply some correction factors to eq. (1) for $0 \le R \le 0.75$:

$$\frac{Q}{\lambda_s \cdot \lambda_{dr} \cdot \lambda_\alpha} = 0.2 \cdot \exp(-2.6 \cdot R), \qquad (2)$$

λ_s takes into account the discrepancies to eq. (1), λ_{dr} corrects for the varying draft (equal to 1 in this paper) and λ_α adjusts for the varying slope angle.

The Q- and R-values calculated for the experimental tests are plotted against (1) and (2) for $0.6 \le R \le 3.5$ in Fig. 7. In addition the 5% lower and upper confidence limits for eq. (1) are plotted.

Fig. 7 shows that the data points for the non-composite slope of 30° (data 30°) are in good agreement with eq. (1) (R^2-value of 0.81). This is due to the fact that similar geometries to C and D (Table 1) were included when deriving eq. (1). The other geometries are not included. Furthermore, in some of the tests for 40° and 50° the limits of eq. (1) are violated. For a number of combinations of the test parameters (when looking at the composite slopes), $\cot \alpha < 1$ and $\xi_{m-1,0} > 5$. The data points for 40° (data 40°) are below the curve corresponding to (1) (R^2-value of 0.19). The agreement for 50° (data 50°) is even worse (R^2-value of -3.51). It is logical that the Q-value corresponding to a certain R-value decreases when the slope approaches a vertical wall.

Fig. 8 shows the (Q,R)-values of the experimental tests against eq. (2) for $0 \le R \le 0.6$. The data points follow the same non-linear trend as eq. (2) but are below the curve corresponding to eq. (2). A possible explanation is that eq. (2) is derived, based on tests with geometries that had a limited draft. When the slope is not extending to the bottom, reflection is lower and therefore overtopping is higher.

A comparison between the subsets of data points within the data set (e.g. groupiness) is not carried out here and will be reported elsewhere. The goal is to validate the test results against the empirical formulae. Fig. 7 and Fig. 8 show that the average overtopping discharges are in good agreement with empirical formulae found in literature.

5 Experimental model – results individual volumes

The intended outcome of the validation tests are the individual overtopping volumes, wave by wave. These volumes can be either deduced from the cumulative curve or from the time-differentiated curve (section 2). When looking at a theoretically expected cumulative curve (Fig. 9), every increase (jump) in the curve corresponds to a wave overtopping the reservoir. The difference between the water mass in the reservoir after each jump and the water mass before each jump is then equal to the volume of overtopped water corresponding to an overtopping wave. The moments when overtopping occurs at the crest of the slope can be derived from the signal of the overtopping detection system.

A theoretically expected time-differentiated curve is shown in Fig. 10. The volume of water that entered the reservoir for every overtopping wave (peak) then equals the surface below that peak.

However, the measured curves look different from Fig. 9 and Fig. 10. In this paper these curves are given for a test with regular waves W3 and geometry B1 as this is the test that has been simulated in the numerical model. In the following paragraph, the chosen strategy to determine the individual overtopping volumes of the experimental test results is explained for this specific test B1-W3(regular).

The measured signal of the weigh cell is shown in Fig. 11. Although the intended incident waves are regular and should give a regular overtopping pattern, the signal of the weigh cell is not completely regular. This is due to the non-linearity of the waves in the flume, the absence of active wave absorption and the presence of long waves in the flume.

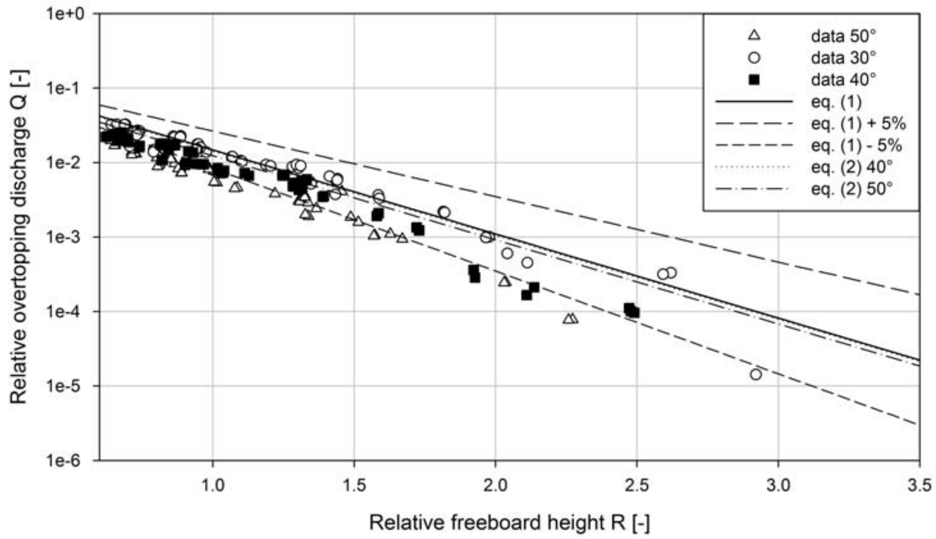

Figure 7: Comparison test results with empirical formulae for $0.6 \le R \le 3.5$.

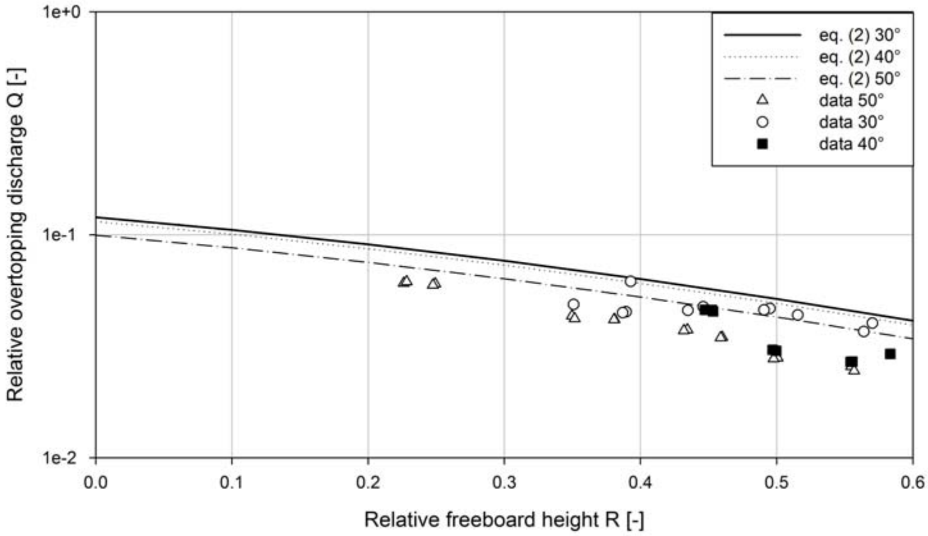

Figure 8: Comparison test results with empirical formulae for $0 \le R \le 0.6$.

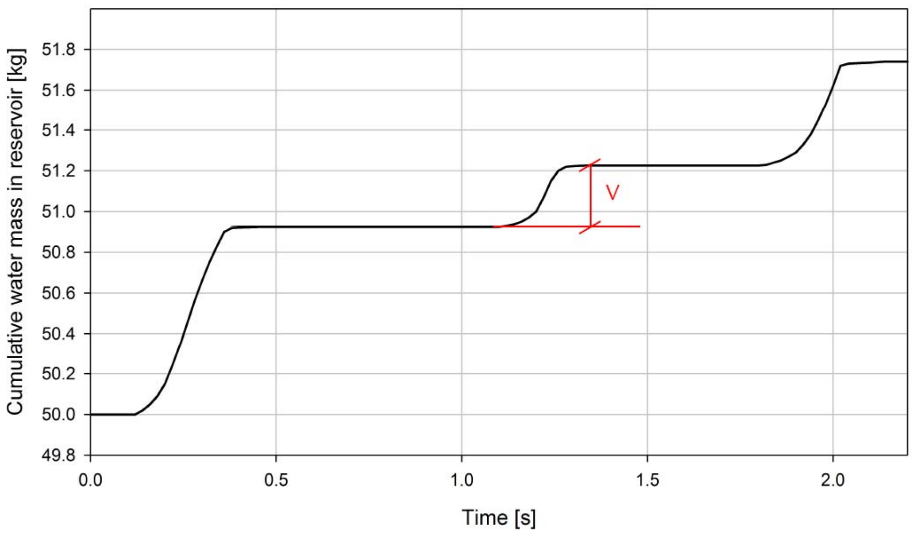

Figure 9: Theoretically expected cumulative curve for overtopped volumes.

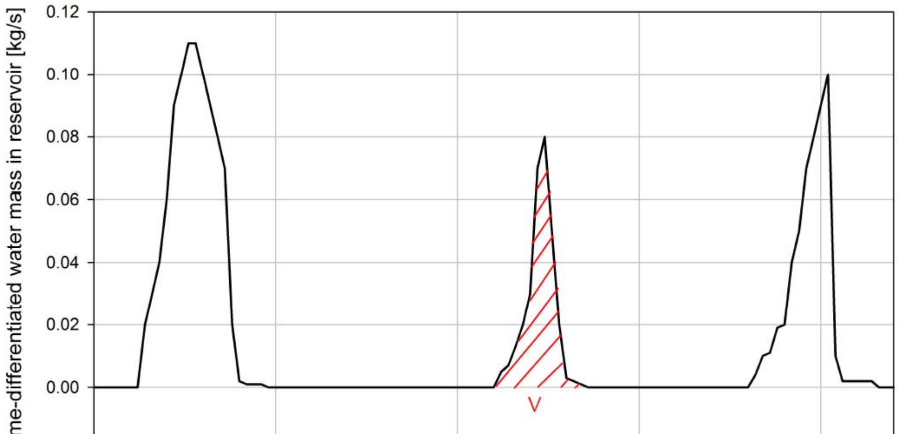

Figure 10: Theoretically expected time-differentiated curve for overtopped volumes.

For regular waves, the intended outcome is an average individual overtopping volume. The influence of these factors causing the non-regularities on this outcome is considered to be limited. Initially, the same method is used as when determining the average overtopping discharges. The pump characteristic for the tests is shown in Fig. 12. Smoothing of the weigh cell signal is applied to obtain a better distinguishing of the individual volumes in its derived curves. The smoothing parameters are determined by using two test cases for which known volumes of water were added to the reservoir at known times and then re-identified from the cumulative curve. Smoothing is also used when determining the average overtopping discharges.

The average individual overtopping volume is determined based on both methods mentioned at the start of this section. Fig. 13 shows the cumulative curve (section 2) for B1-W3(regular). It can be noticed that a dynamic effect is present when the waves fall into the reservoir: a temporary overestimation of the overtopped volume occurs. This is taken into account when determining the individual overtopping volumes by considering a more extended time interval around the overtopping positions. The average individual overtopping volume derived from the cumulative curve for B1-W3(regular) equals **6.73 l.** The corresponding time differentiated curve is shown in Fig. 14. The dynamic effect of the waves entering the reservoir is present as negative troughs. The individual volume of an overtopping wave should be determined as the area below a positive peaks minus the area below the negative peak that follows the positive one.

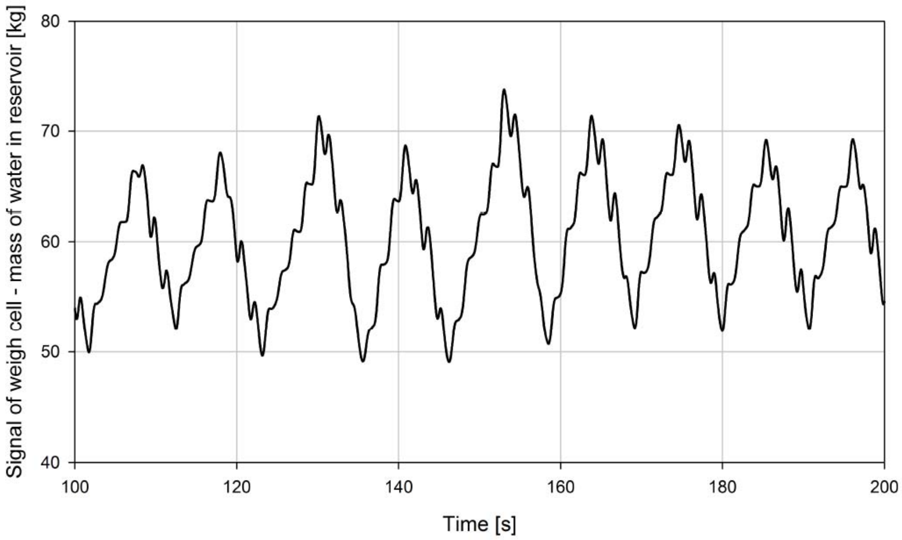

Figure 11: Measured signal weigh cell – geometry B1, regular waves W3.

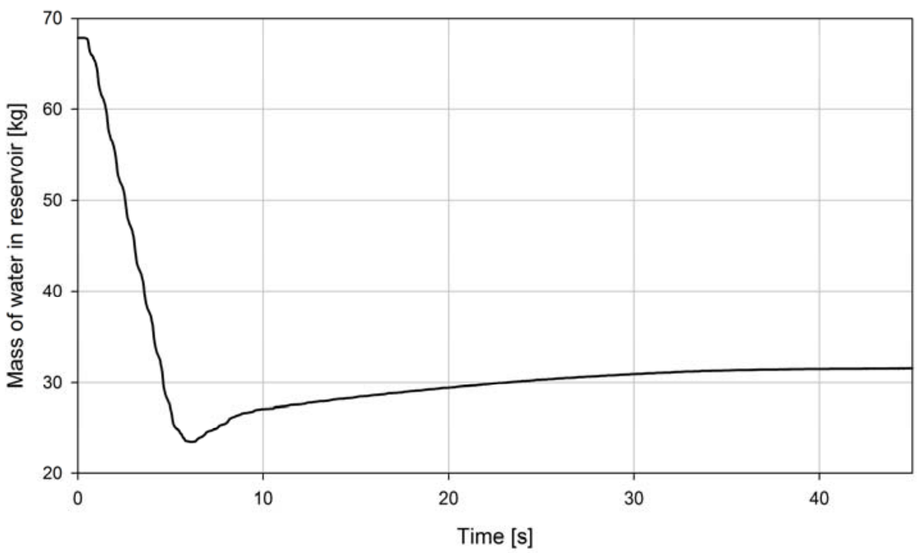

Figure 12: Pump characteristic for validation tests (August 2008 – October 2008).

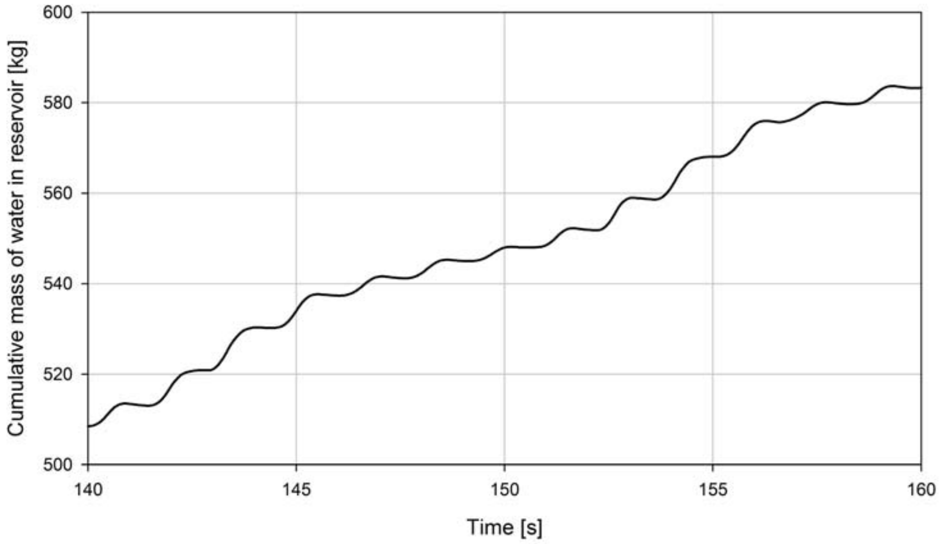

Figure 13: Cumulative signal weigh cell – geometry B1, regular waves W3.

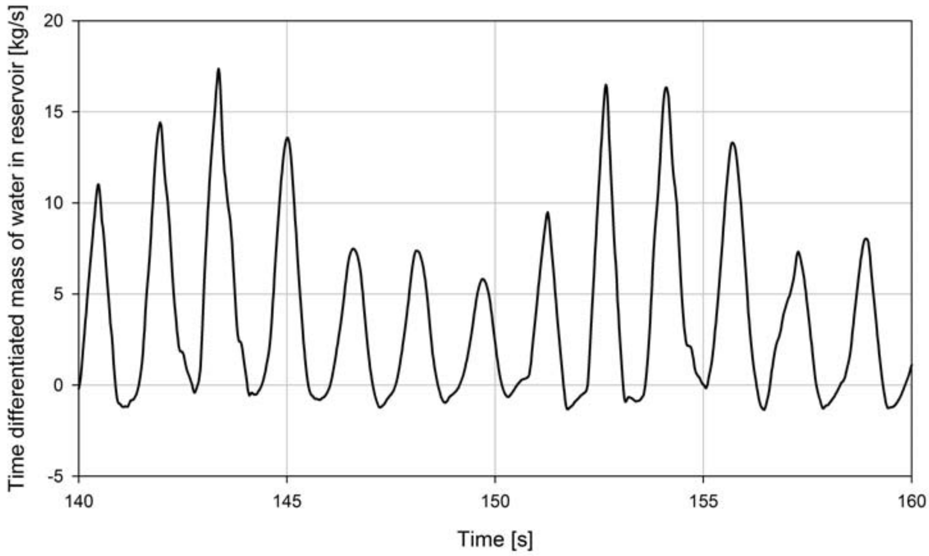

Figure 14: Time-differentiated signal weigh cell – geometry B1, regular waves W3.

However, in general the negative peaks are small and can therefore be neglected. The average individual overtopping volume derived from the time-differentiated curve for B1-W3(regular) equals **6.68 l.** This value is almost identical to the result of the method based on the cumulative curve.

6 Results numerical tool – first comparison with experimental results

A first comparison between numerical and experimental results has been carried out for B1-W3(regular). In particular, the average individual overtopping volume has been derived numerically and compared to the experimental results. The basic components of the numerical wave flume are described in section 3. The position of the source generating the waves is determined by the position of the wave gauges used for reflection analysis (three WGs are used in WaveLab). In the test set-up two sets of wave gauges are available: WG1, WG2, WG3 and WG6, WG7, WG8. Reflection analysis gives the incident wave characteristics for the position of WG1 or WG6. The mass source has been put at a distance of the structure equal to that of WG6. Validation of the incident wave characteristics at the position of WG1 can then be carried out. The corresponding water depth at the position of WG6 for the considered test is 0.57 m. The time-averaged incident wave characteristics used for the mass source generation are: wave height 0.1185 m and wave period 1.533 s. A simulation of 20 s has been carried out. The dimensions of the numerical wave flume are 15 m x 1 m x 1 m (LxBxH). The mass source is positioned 9 m from the left boundary (x = 0 m). A sponge layer with a length of 8 m is present in front of the left wall. A reservoir of approximately 3 m length is present behind the structure. It contains a mass sink at its bottom to make sure the water level in the reservoir does not increase too much so that it would prevent the waves from overtopping. A sponge layer behind the structure is not required here. The source positioned below the wave generating source to correct for the overtopped water has been disabled, i.e. it's mass source rate has been set to 0 kg/s. Fig. 6 gives an overview of the components used in the numerical wave flume. The mesh consists of 800x1x200 cells (XxYxZ). A 2D calculation has been carried out, using one cell in the Y-direction. According to [9], the overtopping discharges derived from a numerical model depend on the choice of the computational grid. The instructions given in [9] are taken into account as much as possible, e.g. the still water level coincides with the cell boundary and the mesh is fine enough to model the geometry correctly (Fig. 15).

The results of the simulation are given below.

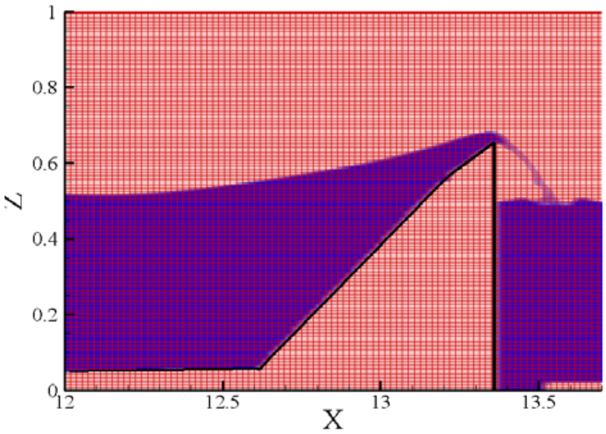

Figure 15: Grid and geometry for B1-W3 in FLOW3D.

Fig. 16 shows the total wave elevations at two different positions in the wave flume at the right side of the mass source. The two curves show the presence of a quasi-standing wave pattern in the numerical wave flume. This phenomenon also appeared in the experimental wave flume. The slope of the structure is quite steep and the corresponding reflection coefficients are within the range of 60%-90%. For the specific test that is emphasized here, a reflection coefficient of 75 % has been derived from the experimental test results. Long waves are not visible in Fig. 16 as the simulation time is too short for the long waves to appear.

This is also the reason why an accurate reflection analysis to determine the incident waves at the position of WG1 (corresponding to x=10.5 m) can not be carried out. Therefore, longer simulations are required.

The numerical tool includes the possibility to install a surface ("baffle") at a certain position to derive the flux ($m^3/s/m$) through that surface in time (baffle). A baffle has been installed at the crest of the slope. The flux through the baffle as a function of time is shown in Fig. 17, in which the vertical axis has been transformed to kg/s (multiplying with the width of the physical wave flume and the density of water 1000 kg/m^3). Every peak represents an overtopping event. Different zones can be distinguished in Fig. 17. The first two peaks correspond to overtopping waves that are in the transition zone between calm water and the intended waves. The three peaks that follow can be seen as overtopping events from the intended waves, as the decrease in water level will be limited in that period of time. After these three peaks, the decrease in wave height becomes significant. A solution to reduce this effect is being developed. A comparison with results of the experimental model can be carried out based on the three peaks between 7 s and 11 s (Fig. 17). When comparing these three peaks with the peaks in Fig. 14, it can be concluded that there is a very good agreement between the experimental and numerical model. On average the top values of the peaks in both the numerical and the experimental model correspond to approximately 8 kg/s. The average individual volume corresponding to one wave derived from the numerical tool is thus **6.24 l**. This corresponds to a small underestimation of the experimental result: $V_{num}/V_{phys\_average} = 0.93$.

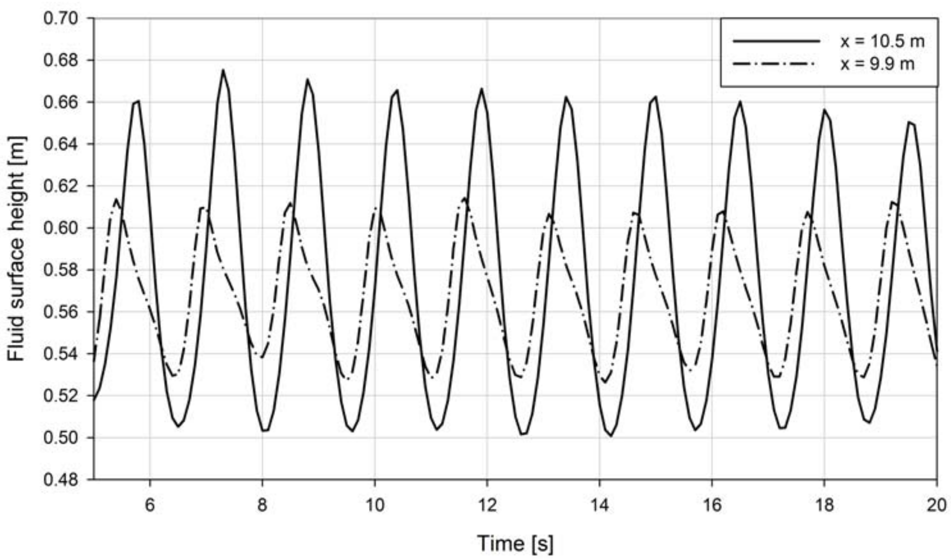

Figure 16: Fluid surface heights at positions x = 9.9 m and x = 10.5 m.

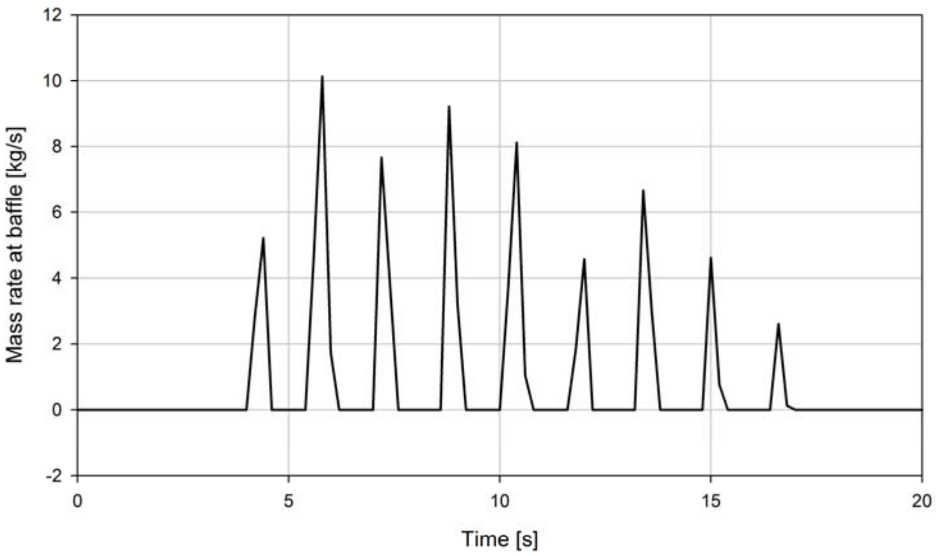

Figure 17: Mass rate through the baffle at crest of the structure.

7 Conclusions

Experimental model tests have been carried out to validate the ability of a commercial CFD-solver to give accurate results for individual overtopping volumes at a WEC. The set-up has been described and the experimental results for average overtopping discharges have been validated with empirical formulae from literature. The strategy to determine the individual overtopping volumes has been explained and illustrated with a specific test with regular waves. As a first validation of the numerical tool, this test has been modeled in the CFD-program. Comparable results are achieved for the average individual overtopping volume.

Acknowledgements

The authors would like to acknowledge the suggestions by D. Vanneste for the numerical part of this paper. The technicians at AWW-UGent and Aalborg University are acknowledged for their help with the experimental test set-up. The Fund for Scientific Research-Flanders (FWO-Vlaanderen) is granted for funding the research.

References

[1] L. Victor, P. Troch and D. Vanneste. Experimental and numerical study of the hydrodynamic behavior of wave energy converters based on wave overtopping. In *Proc. 2nd International Conference on Ocean Energy (ICOE)*, Brest, France, 2008.

[2] Mansard E. and E. Funke. The measurement of incident and reflected spectra using a least square method. In *Proc. 17th International Conference on Coastal Engineering (ICCE),* Sydney, Australia, 1980, Vol. 1. pp. 154-172.

[3] FLOW3D®: www.flow3d.com.

[4] EurOtop-Team. *Wave Overtopping of Sea Defenses and Related Structures: Assessment Manual*, 2007.

[5] J.P. Kofoed. *Wave overtopping of Marine Structures - Utilization of Wave Energy.* PhD thesis, Aalborg University, 2002.

[6] J.W. Van der Meer and J.P.F.M. Janssen. Wave run-up and wave overtopping at dikes and revetments. Technical Report no. 485, Delft Hydraulics, August 1994.

[7] M.R.A. van Gent. Wave runup on dikes with shallow foreshores. *Journal of Waterway, Port, Coastal and Ocean Engineering*. Vol. 127(5), pp.254-262, 2001.

[8] J.W. Van der Meer, H. Verhaeghe and G.J. Steendam. Final report on wave overtopping at coastal structures, CLASH WP2 report, Infram, Marknesse, The Netherlands, 2005b.

[9] P. Troch, J. De Rouck and H. Schüttrumpf. Numerical simulation of wave overtopping over a smooth impermeable sea dike. *Advances in Fluid Mechanics IV*. Vol. 36, pp.715-724, 2002.